PCCP

Nanoparticle Assembly Following Langmuir-Hinshelwood Kinetics on a Langmuir Film and Chain Networks Captured in LB Films

Journal:	*Physical Chemistry Chemical Physics*
Manuscript ID:	CP-ART-01-2015-000606
Article Type:	Paper
Date Submitted by the Author:	30-Jan-2015
Complete List of Authors:	Maganti, Lasya; University of Hyderabad, School of Chemistry Jash, Madhuri; University of Hyderabad, School of Chemistry Nair, Anju; University of Hyderabad, School of Chemistry Radhakrishnan, T.P; University of Hyderabad, School of Chemistry

Cite this: DOI: 10.1039/c0xx00000x

www.rsc.org/xxxxxx

ARTICLE TYPE

Nanoparticle Assembly Following Langmuir-Hinshelwood Kinetics on a Langmuir Film and Chain Networks Captured in LB Films

Lasya Maganti, Madhuri Jash, Anju Nair and T. P. Radhakrishnan*

Received (in XXX, XXX) Xth XXXXXXXXX 20XX, Accepted Xth XXXXXXXXX 20XX

DOI: 10.1039/b000000x

Langmuir-Blodgett (LB) technique is an elegant protocol for the steered assembly of metal nanoparticles, the deposition pressure serving as a convenient parameter to tune the assembly. Adsorption of nanoparticles from the subphase to the air-water interface can provide further control on the process. Citrate-stabilized gold nanoparticles in the aqueous subphase are shown to assemble into extended 2-dimensional chain networks following adsorption on a cationic amphiphile Langmuir film at the air-water interface. Kinetic investigations show that the process can be visualized as a surface-catalyzed reaction and explained in terms of the Langmuir-Hinshelwood mechanism. The LB deposition proves to be a unique route to capture the reaction product together with the amphiphile film. The deposition pressure is used to tune the density of nanoparticle chain networks in the LB film, and their optical extinction spectrum. The unusual blue shift of the extinction observed with increasing deposition pressure is attributed to the impact of the amphiphile monolayer environment. The extent of formation of the chain network is analyzed in terms of the pathways in the corresponding graph representation, and shown to scale with the deposition pressure. The current investigation highlights the use of a charged monolayer as a heterogeneous catalyst surface, provides fundamental insight into the kinetics of nanoparticle assembly at interfaces, and demonstrates the utility of the LB technique in tuning the formation of 2-dimensional nanoparticle chain networks.

Introduction

A key attribute of nanoparticles of noble metals such as gold and silver is their optical response arising from the localized surface plasmon resonance (LSPR).[1,2] The application potential of this unique property stems not only from the associated large oscillator strength, but also its sensitivity to the size/shape of the particles, the dielectric environment and the interactions in particle assemblies. The latter is particularly relevant as a wide range of non-covalent interactions and principles of supramolecular organization can be brought to bear upon the assembly and thus tune the optical responses, without the need to modify the synthesis or growth of the nanoparticles. Metal nanoparticles have been assembled as dimers,[3] larger aggregates,[4] chains or polymers,[5,6] arrays,[7] monolayers[8] and networks.[9] Networks are of special interest because of their relevance in percolation problems,[10,11] in addition to the tunability of optical responses that can be exploited in various applications.

A systematic approach to the generation of nanoparticle networks would involve a controlled assembly induced by non-covalent forces. Gold nanoparticle chain networks have been implicated as intermediates in the formation of spherical nanoparticles by the Turkevich method, suggesting a mechanism different from the La Mer nucleation-growth model.[12] Chain networks form through dipolar interactions triggered by an asymmetric distribution of adsorbed charges[13] or ligand segregation[14] on the nanoparticle surface. Metal nanoparticle networks can be generated using selected combinations of ligands and metal ions as in the case of peptide and 3-mercaptopropionic acid functionalized gold nanoparticles with mercuric and cupric ions respectively.[15,16] Examples of template-mediated network formations include the DNA-directed assembly of trimethyl(mercaptoundecyl)ammonium monolayer coated gold nanoparticles[17] and the organization of gold nanoparticles on peptide nanofibers[18,19] and polyelectrolytes.[16,20] An interesting case of nanoparticle network formation exploits dielectrophoresis forces induced by a non-uniform electric field.[21]

The Langmuir-Blodgett (LB) technique commonly used to fabricate mono and multilayer films of amphiphilic molecules, through steered rather than self-assembly, can be used to organize metal nanoparticles and nanowires in ultrathin films.[22] An obvious approach is to spread amphiphile-capped nanoparticles at the air-water interface to form a monolayer and transfer it as an LB film. Dodecanethiol is a popular choice for the amphiphile;[23-26] other capping agents include amphiphiles with ammonium headgroups,[27,28] mixed amphiphile systems,[29,30] liquid crystalline molecules[31] and polymers.[32] A different approach involves the introduction of the metal nanoparticles in the aqueous subphase which then interact with the amphiphile monolayer and form networks. An amphiphilic derivative of tetrathiafulvalene-tetrafluorotetracyanoquinodimethane complex spread at the air-

water interface and hybridized with gold nanoparticles formed LB films with nanowire structures exhibiting electrical conductivity.[33] Adsorption of negatively charged gold nanoparticles on a Langmuir film of dioctadecyldimethyl-ammonium bromide at the air-water interface has been shown to be influenced by the electrostatic interaction between the monolayer and the nanoparticles, flow of water in the subphase and the mass of the nanoparticles.[34] Studies on the interaction of positively charged poly(allylamine hydrochloride)-functionalized and negatively charged citrate-capped gold nanoparticles with different lipids in Langmuir monolayers have revealed the crucial role of the charge on the capping agent and the impact on the elasticity of the monolayers.[35] Dendritic nanogold aggregates were generated by salt-induced assembly of gold nanoparticles mediated by the polyacrylamide - cetyltrimethylammonim bromide complex at the air-water interface.[36] Gels of gold nanoparticle aggregates formed in mixed Langmuir films of stearic acid and octadecylamine and transferred as LB films, developed dendrite-like organic crystals coated with the nanoparticles.[37] LB film formed with precursor ions adsorbed from the subphase have been used for the subsequent generation of nanoparticle networks.[38] An approach investigated in our laboratory involved dipping the LB film of *N*-*n*-octadecyl-4-[2-(4-dimethylaminophenyl)ethenyl]pyridinium bromide ($ODEP^+Br^-$) in a solution of citrate-stabilized gold nanoparticles whereupon the nanoparticles get adsorbed on the LB film.[39]

Possibility of controlling the aggregation of amphiphilic molecules to varying extents by tuning the deposition pressure makes the LB method a versatile technique for the steered assembly of molecules. The examples of nanoparticle assembly cited above demonstrate the interaction between the Langmuir films and the metal nanoparticles in the subphase; however, they do not exploit the LB technique to tune the nanoparticle assembly through the process of adsorption on and mediation of the Langmuir film. Modeling the assembly and probing its kinetics are of fundamental interest. We have explored the interaction of negatively charged citrate-stabilized gold and silver nanoparticles present in the aqueous subphase with the Langmuir film of the amphiphiles, $ODEP^+Br^-$ and N-*n*-octadecyl-4-dimethylamino-pyridinium bromide (ODP^+Br^-) possessing cationic head groups. Detailed studies on the prototypical combination of gold nanoparticles and $ODEP^+Br^-$ are presented in this paper; parallel observations on silver nanoparticles/$ODEP^+Br^-$ and gold nanoparticles/ODP^+Br^- combinations are added in the Supporting Information.[40] The nanoparticles in solution are found to assemble into extended network structures through the mediation of the monolayer at the air-water interface; the process is modeled as a surface-catalyzed reaction following Langmuir-Hinshelwood kinetics. The 2-dimensional nanoparticle networks along with the amphiphile monolayer can be captured through LB film transfer. The extent of network formation, quantified in terms of the number and length of paths in the corresponding graph representation, is shown to increase with the deposition pressure and exhibit unusual trends in their optical responses.

Results and Discussion

Citrate-stabilized gold nanoparticles were prepared using a slightly modified Turkevich method.[41] Aqueous solution of the

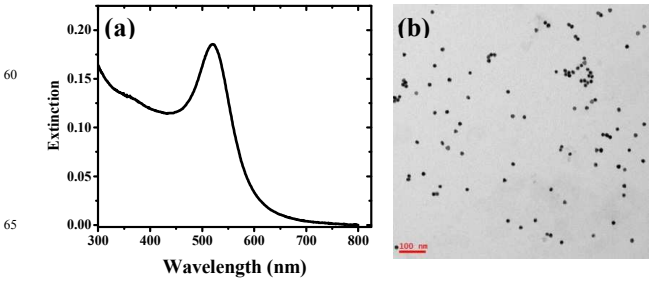

Figure 1. (a) LSPR extinction spectrum and **(b)** TEM image (scale bar = 100 nm) of the gold nanoparticles used in the study.

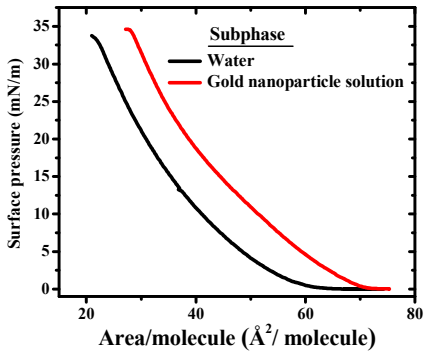

Figure 2. Pressure-area isotherms of $ODEP^+Br^-$ monolayer at the air-water interface, with pure water and 0.011 mM gold nanoparticles solution as the subphase.

nanoparticles shows the typical LSPR extinction peak at 520 nm; the TEM image of a drop of solution evaporated on the grid reveals nearly spherical particles with diameters in the range 13 – 15 nm (Fig. 1). Solution of $ODEP^+Br^-$ in chloroform shows the characteristic intramolecular charge transfer absorption with λ_{max} ~ 498 nm.[42] π-A isotherm of $ODEP^+Br^-$ at the air-water interface is shown in Fig. 2; the molecular area estimated by extrapolating the high surface pressure part is ~ 40 $Å^2$/molecule, suggestive of a nearly vertical disposition of the amphiphile headgroup.[43] The tendency of $ODEP^+$ amphiphile to aggregate at the air-water interface is well established.[44] Electronic absorption of the monolayer LB film of $ODEP^+Br^-$ is quite sensitive to the extent of aggregation; in the present study, the spectrum of the film deposited at 30 mN/m shows peaks at 464 nm and 270 nm (Fig. 3) typical of the chromophore monomers.[45]

π-A isotherm of $ODEP^+Br^-$ monolayer spread on the aqueous solution of gold nanoparticles is also shown in Fig. 2. The isotherm shows a clear shift to higher areas and indicates an extrapolated area of ~ 50 $Å^2$/molecule. This is indicative of the interaction between the cationic amphiphiles and the citrate-stabilized nanoparticles; either the nanoparticles are inserting partly into the monolayer causing it to expand, or the head groups adopt a more tilted orientation occupying more of the surface area. Extinction spectrum of a 2-layer LB film deposited at a surface pressure of 30 mN/m is shown in Fig. 3. No significant absorption is visible at ~ 460 nm where the $ODEP^+$ monomer absorbs. However, the peak observed at 265 nm is characteristic of $ODEP^+$ and the shoulder at ~ 350 nm is similar to that observed in $ODEP^+$ based LB films,[44,45] attributed to the chromophore dimer.[42] The other peaks in the spectrum arise due to the gold nanoparticles; interestingly, the LSPR peak at ~ 520 nm due to the isolated nanoparticles is considerably diminished

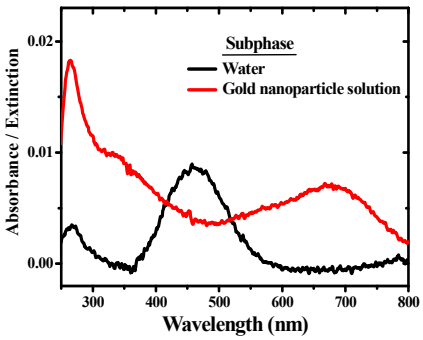

Figure 3. Absorption / extinction spectra of LB films of $ODEP^+Br^-$ deposited at 30 mN/m pressure, from subphases of pure water and 0.011 mM gold nanoparticles solution.

and a prominent one appears at ~ 685 nm suggestive of nanoparticle assembly; the tail extends into the near infrared region. Before exploring the LB films further, we have probed deeper into an interesting observation of significant changes occurring in the gold nanoparticle solution subphase itself, when the amphiphile monolayer is formed at the air-water interface.

When the $ODEP^+Br^-$ monolayer compressed to the close-packed condensed phase (typically at pressures > 20 mN/m) was maintained for several minutes, the subphase color was found to gradually change from ruby red (typical of isolated gold nanoparticles) to purple, violet and eventually blue (typical of aggregated nanoparticles). The nanoparticle solution without the monolayer at the surface is perfectly stable for several days with no visible color change, as expected; it may be stressed also that even if the amphiphiles are spread on the surface, but maintained at ~ 0 mN/m surface pressure (in the so-called gas phase), the subphase shows no noticeable change for several hours. With the compressed monolayer, if the solution at any stage of aggregation is separated from the monolayer, it remains stable with no further color change, for extended periods of time. These observations prove the critical role of the monolayer at the air-water interface in mediating the nanoparticle assembly. Compared to surfactants such as those with ammonium headgroups that can form micelles in water,[46] $ODEP^+$ with its extended aromatic head group is likely to be far less soluble, and at the very low concentrations present at the interface, unlikely to form micelles in the aqueous medium. The π-A isotherms (Fig. 2) indicate good stability of the monolayer at the air-water interface; the improved stability with the gold nanoparticle solution as the subphase[40] precludes the possibility of the nanoparticles enhancing the solubility of the monolayer. All these suggest that the nanoparticle assembly occurs catalytically at the air-water interface. It is interesting to view this in the context of the condensation of monolayers at the air-water interface in a manner similar to colloidal coagulation[47] and the competitive adsorption of proteins and lipids at the air-water interface[48] influenced by ions with different valencies. Compared to the well-studied cases of nanoparticle aggregation by agents added in solution, the assembly mediated by an insoluble monolayer at the air-water interface is likely to be more controlled, and result in aggregates that when back in the aqueous phase, will be free of the aggregating agent. We have probed this situation in detail.

Citrate-stabilized gold nanoparticle solution with different concentrations was taken in a petri-dish. A solution of $ODEP^+Br^-$

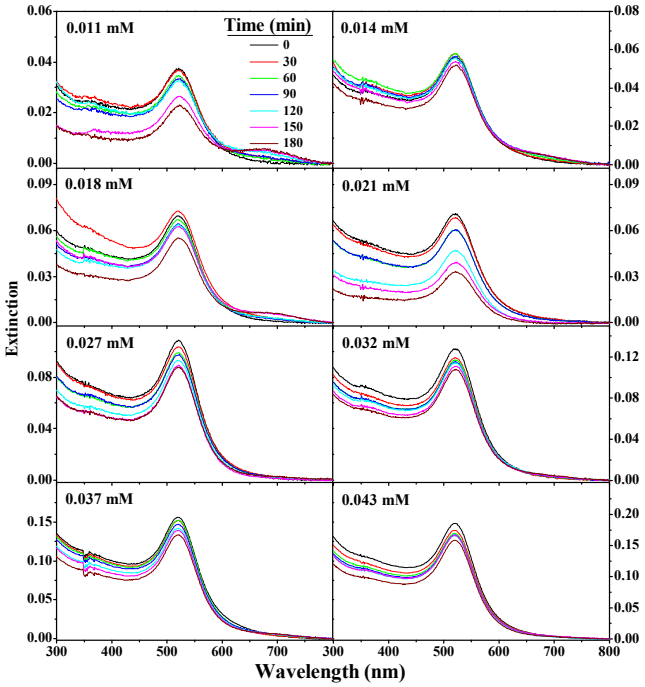

Figure 4. Temporal evolution of the extinction spectra (corrected for scattering) of the gold nanoparticle solutions with different initial concentrations, and an $ODEP^+Br^-$ monolayer at the surface.

in chloroform containing the number of molecules required to form a monolayer on the solution in the petri-dish was spread slowly and the chloroform allowed to evaporate. Color changes of the subphase were monitored by recording the extinction spectrum of small samples withdrawn periodically. Time evolution of the spectra for different initial concentrations of the gold nanoparticles are shown in Fig. 4. At low initial concentrations (0.01 – 0.02 mM), the peak at ~ 520 nm is found to decrease steadily and the peak at ~ 685 nm to increase concomitantly. The isosbestic point near 605 nm is indicative of a direct conversion process between the 'reactant' and 'product'. With intermediate initial concentrations (0.02 – 0.03 mM), even though the peak at ~ 520 nm decreases steadily, no clear peak emerges at higher wavelength. On the other hand, the baseline of the spectrum rises suggesting increasing scattering effects.[40] At still higher initial concentrations (0.03 – 0.04 mM), growth of a small peak at the higher wavelength can be discerned, though it is partly masked by the high scattering. The raw spectra were corrected for scattering effects and deconvoluted to extract the intensity of the extinction with λ_{max} ~ 520 nm. Intensity of this peak at t = 0 min scales linearly with the initial concentration of the gold nanoparticle solution as expected (Fig. 5a); standard deviations determined from multiple runs are shown. For each initial concentration, a plot of the nanoparticle concentration (determined from the intensity) against time provides the rate of the assembly process from the slope of the early (typically up to 120 min) linear part.[40] Dependence of the rate on the initial concentration is shown in Fig. 5b; it increases, then levels off and finally decreases with increasing concentration. Surface reactions that follow the Langmuir-Hinshelwood mechanism typically exhibit rates increasing with concentration in the low

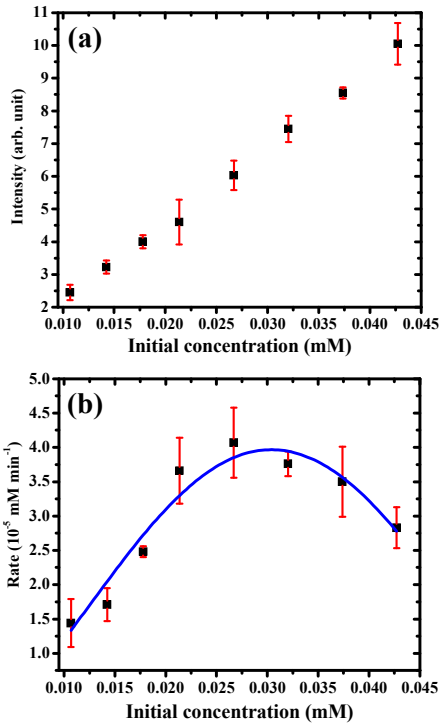

Figure 5. Plot of **(a)** the intensity of the extinction due to isolated gold nanoparticles (with λ_{max} ~ 520 nm) at t = 0 min versus the initial concentrations of gold nanoparticles, and **(b)** the rate of nanoparticle assembly versus the initial concentration; standard deviations and fit to the rate expression in Scheme 1 are indicated.

concentration regime. At higher concentration levels, the rate becomes constant if the reacting species alone is involved in the adsorption process, but decreases if a second species competes for the adsorption sites on the surface. In the present case, citrate ions present in large excess in the gold nanoparticle solution could potentially be adsorbed strongly on the cationic amphiphile Langmuir monolayer hindering the nanoparticle assembly process. Adsorption of the citrate-stabilized gold nanoparticles from the subphase on to the monolayer at the air-water interface and their subsequent assembly into chains are shown schematically in Fig. 6a. The plausible mechanism along with the resulting kinetic equations are presented in Scheme 1. The critical assumptions in the proposed mechanism are : (i) the assemblies arise from gold nanoparticles adsorbed on the Langmuir film following the Langmuir adsorption isotherm, the positively charged film screening the repulsion between the negatively charged nanoparticles, (ii) the rate determining step in the assembly is the dimerization of the nanoparticles with the subsequent steps including the desorption being fast, and (iii) the citrate ions which are in a constant and excess proportion with respect to the gold nanoparticles (as a fixed ratio between citrate and gold is used in the nanoparticle synthesis itself) are potential poisons for the adsorption sites on the Langmuir film. The first assumption is validated by the observation that the nanoparticle assembly or aggregation occurs only when the Langmuir film is present at the solution surface. The second assumption is based on the likelihood of the chain formation being triggered by the distortion of the ligand environment and the resulting asymmetry around the nanoparticle due to the dimerization. Interaction of

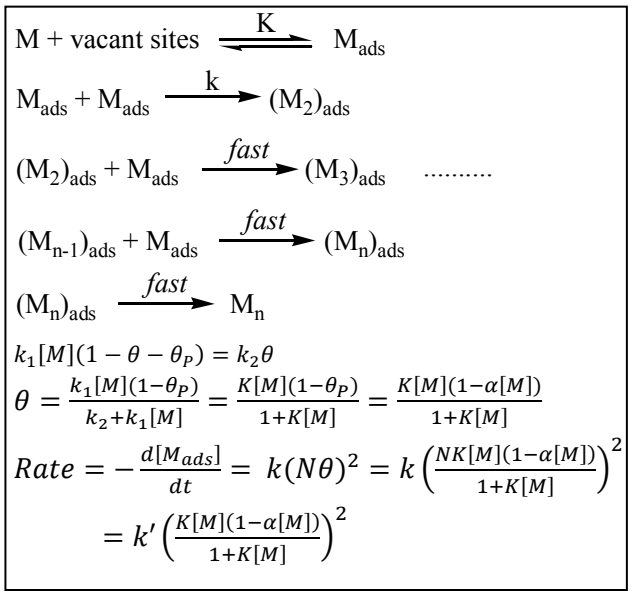

Scheme 1. Mechanism involving the adsorption of isolated gold nanoparticles (M) with equilibrium constant K, dimerization as the rate determining step with rate constant k, and the subsequent fast steps. Kinetic equations that lead to the final rate expression involving the fraction of surface sites occupied by the gold nanoparticles and the citrate ions, θ and θ_P respectively, the total number of adsorption sites, N, rate constants for the adsorption and desorption of the gold nanoparticles, k_1 and k_2 respectively, and the ratio (α) of θ_P to [M].

citrate with the Langmuir film (exchange between the bromide and citrate ions) is manifested in the π-A isotherm of $ODEP^+Br^-$ on an aqueous solution of sodium citrate, and the related area-time creep plots[40] which clearly show the enhanced stability imparted by the multivalent anion. Control experiments in which a large excess of citrate was added in the gold nanoparticle solution before introducing the amphiphile Langmuir film showed that the rate of nanoparticle assembly is considerably retarded;[40] this forms the basis for the third assumption. Implicit in the equation for the adsorption-desorption equilibrium is the material balance for the surface sites which are either vacant or occupied by the monomer, M or the poison, P. The resulting rate expression shows that the rate would increase as $[M]^2$ at low concentrations (K[M], α[M] << 1) and decrease due to the dominant $(1 - \alpha[M])^2$ term at high concentrations. Fig. 5b shows that the trend in the rates observed is explained quite satisfactorily by the rate expression in Scheme 1; the parameters which provided the best fit are: the equilibrium constant for the Langmuir adsorption of the nanoparticles, K = 0.175 mM^{-1}, the pseudo rate constant for the dimerization process, k' = 5.63 mM min^{-1} (the true rate constant is not estimated as the exact number of adsorption sites is not known) and the ratio between the fraction of the adsorption sites poisoned by the citrate and the nanoparticle concentration, α = 16.4 mM^{-1}; the correlation coefficient for the fit is 0.94.

The experiment described above shows that the gold nanoparticle assembly occurs at the Langmuir film, in a process akin to surface-catalyzed reactions. The LB films (the cationic amphiphile monolayer with the negatively charged nanoparticle assemblies) transferred at different surface pressures demonstrate how the density of amphiphiles in the 2-dimensional ultrathin

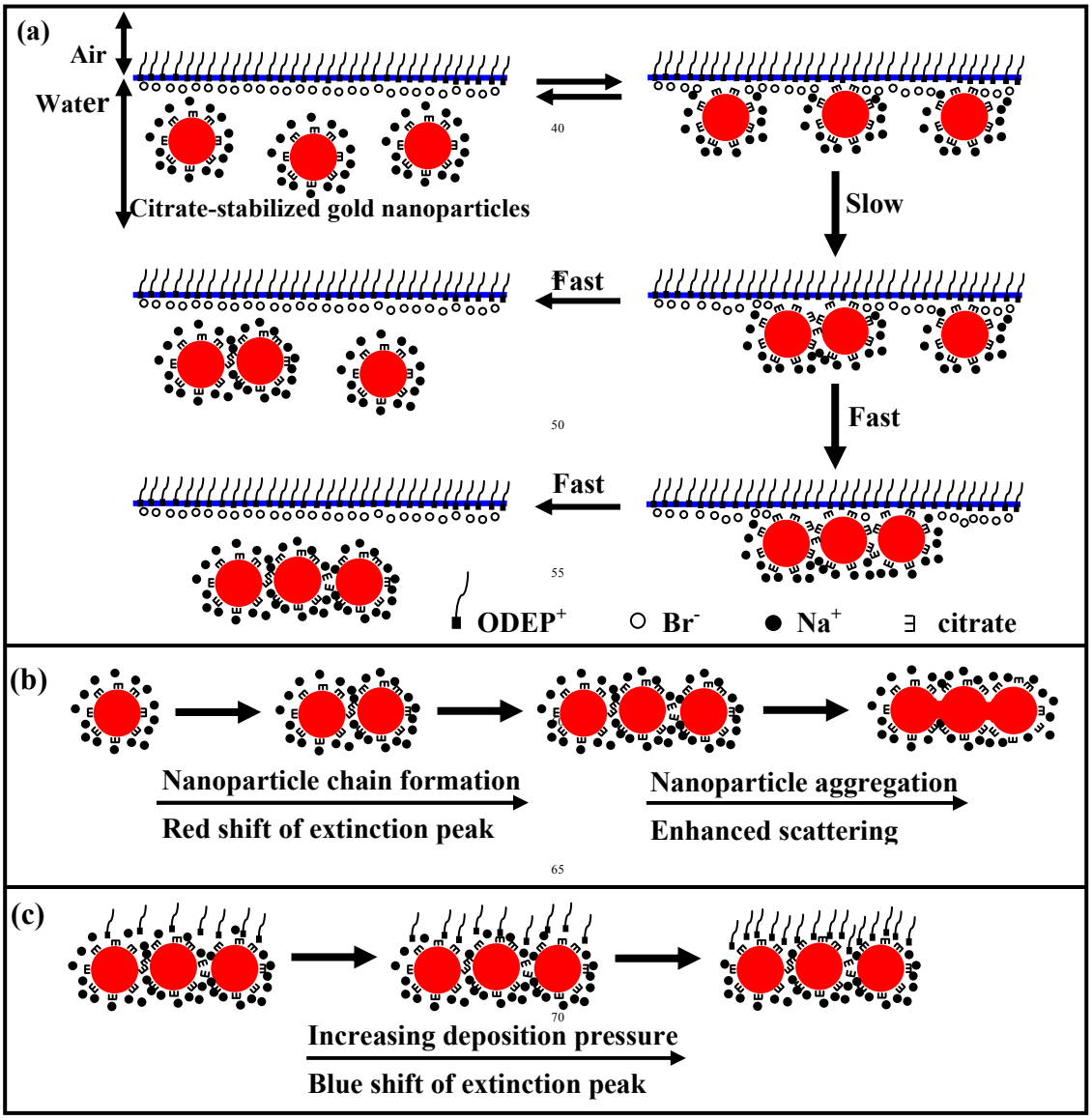

Figure 6. Schematic models of **(a)** $ODEP^+Br^-$ at the air-water interface with citrate-stabilized gold nanoparticles in water and the formation of nanoparticle chains through the mediation of the cationic amphiphile layer at the interface, **(b)** red shift of extinction peak and increased scattering due to nanoparticle chain formation and aggregation, and **(c)** blue shift of extinction peak with increasing deposition pressure, due to the progressive replacement of Na^+ ions by $ODEP^+$ around the gold nanoparticle chains (figures not to scale).

film impacts upon the extent of nanoparticle assembly. Extinction spectra of 2-layer LB films deposited at different pressures, with 0.011 mM solution of gold nanoparticles in the subphase are collected in Fig. 7. As in Fig. 4, the spectra show the prominent peak due to the nanoparticle assemblies; in addition, the absorption due to $ODEP^+Br^-$ is visible. The intensity increases with the surface pressure indicating increasing density of amphiphiles as well as nanoparticles. Significantly, the peak of the LSPR extinction due to the nanoparticle assembly shows a small but definitive blue shift with increasing pressure. Increase in the extent of aggregation or size of aggregates should lead to a red shift of the LSPR peak. The present observation is fundamentally different from the case of LB films of CTAB-stabilized gold nanoparticles that spontaneously aggregate at the air-water interface and exhibit increasing red shift of the extinction which levels off at the higher deposition pressures.[49]

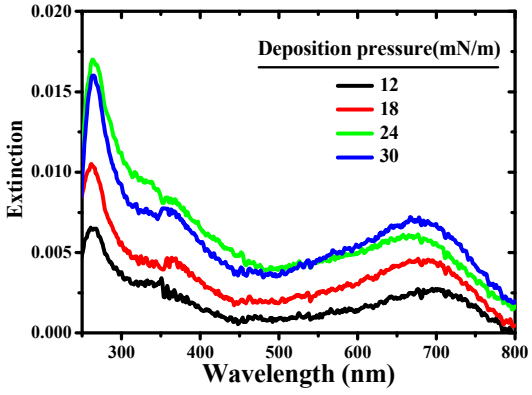

Figure 7. Extinction spectra of LB films of $ODEP^+Br^-$ and citrate-stabilized gold nanoparticles deposited at different surface pressures.

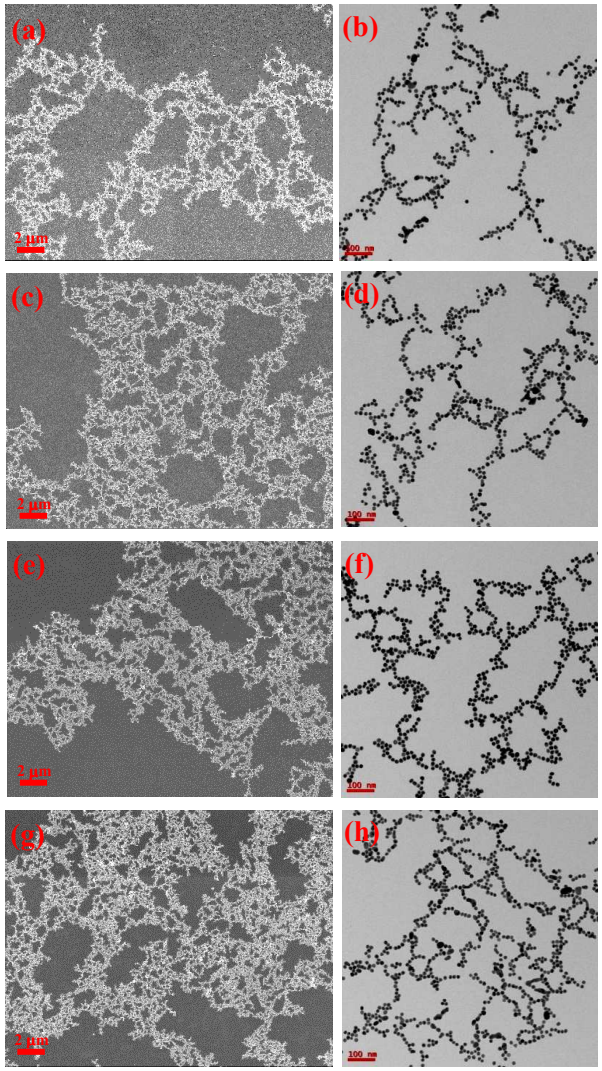

Figure 8. FESEM (left, scale = 2 μm) and TEM (right, scale = 100 nm) images of monolayer LB films of $ODEP^{+}Br^{-}$ and citrate-stabilized gold nanoparticles deposited at different surface pressures: **(a, b)** 12 mN/m, **(c, d)** 18 mN/m, **(e, f)** 24 mN/m, **(g, h)** 30 mN/m.

We return to this point below. FESEM and TEM images of the LB films deposited at different pressures are collected in Fig. 8. The nanoparticles assemble into extended 2-dimensional networks of chains rather than large clusters having multiple neighbours around and above each particle. The two types of images reveal the similarity of the distribution of the chain networks over different length scales and the morphology independent of the substrate used, quartz or copper grid. The average distance between neighbouring particles in a chain is ~ 1 nm. Coupling of the LSPR's of gold nanoparticles at such separations is expected to lead to extinctions with λ_{max} ~ 650 nm[50] consistent with our observation. The extent of connectivity increases in films deposited at increasing surface pressure, however the average separation between the particles remains similar. The unusual blue shift observed in films deposited at increasing surface pressure appears to be a consequence of the dielectric environment. As the surface pressure increases, the number density of the cationic organic amphiphile increases and

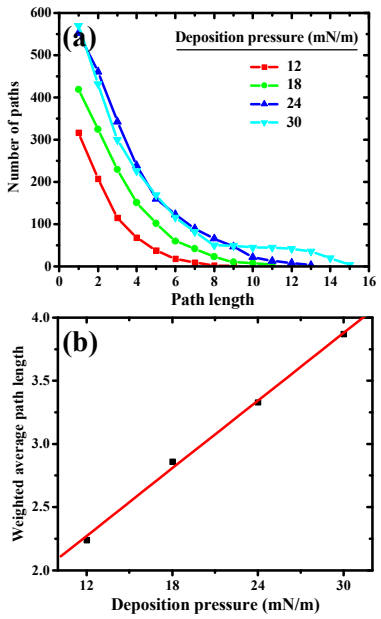

Figure 9. Plot of **(a)** the number of paths with different length in the gold nanoparticle chain networks in the LB films deposited at different surface pressures, and **(b)** the weighted average path length versus the deposition pressure (least square fit line is also shown).

hence the nanoparticle environment will be covered increasingly by these moieties instead of the sodium ions present in the isolated state in solution. Thus the dielectric constant of the local environment possibly decreases leading to a small blue shift.[51,52] Fig. 6b and 6c show schematic models of the nanoparticle assembly. Increase in the scattering effects with high initial concentrations of the gold nanoparticles in the petri-dish experiments described earlier, may be attributed to their possible coalescence (Fig. 6b).[40] Fig. 6c depicts the change in the environment of the nanoparticle assemblies due to the amphiphile layer of increasing density.

The extent of chain network formation was analyzed by counting paths between any two particles (see Experimental section). We have chosen a cut-off distance of 15 nm (between the centres of the nanoparticles) as the criterion for connectivity in the chain network, ensuring that only particles (diameter ~ 14 nm) separated by a distance of ~ 1 nm or less are considered to be linked. The computed chain length distribution in the LB films deposited at increasing surface pressures is shown in Fig. 9a. The lengths of paths formed as well as the number of paths of different length increase as the deposition pressure increases; at the higher pressures, 24 and 30 mN/m, the distributions are similar for shorter paths, but the longest paths emerge only in the networks formed at the highest pressure. The distribution provides a quantitative visualization of the extent of chain network formation in the nanoparticle assemblies and clearly demonstrates the utility of the deposition pressure as a tool to fine-tune it. It is interesting that the weighted average path length scales almost linearly with the deposition pressure (Fig. 9b). Surface coverage of the nanoparticles can be enhanced (Fig. 10) by multiple upward strokes of the substrate through the Langmuir film; there is negligible transfer during down strokes because of the essentially hydrophilic nature of the LB film formed by the

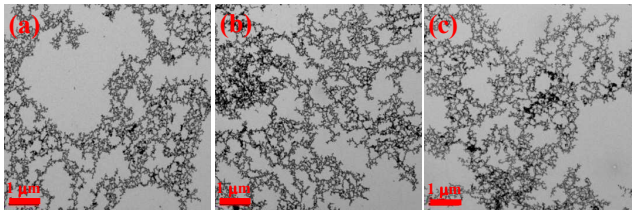

Figure 10. TEM images of LB films of $ODEP^+Br^-$ and citrate-stabilized gold nanoparticles deposited at a surface pressure of 30 mN/m : **(a)** 1-layer, **(b)** 2-layer, **(c)** 3-layer; scale bar = 1 μm.

citrate-stabilized nanoparticles. This method provides a simple method to form monolayer films of gold nanoparticle networks on a desired substrate. Further depositions tend to create multilayer aggregates with particles on top of each other.

It is pertinent to compare the current approach of LB deposition of the amphiphile monolayer – nanoparticle complex following the adsorption of nanoparticles on the Langmuir film, with the earlier method that we have developed[39] involving the dipping of a preformed LB film in a nanoparticle solution. The latter procedure does not provide control on the formation of nanoparticle clusters. Further, the concentrations of nanoparticles in solution required to effect their deposition are far higher than those that we employ in the current approach; control experiments in which pre-formed LB films were dipped in solutions with very low nanoparticle concentrations similar to that used in the subphase in the present study, showed practically no nanoparticle adsorption even after several hours. Thus the adsorption of nanoparticles at the Langmuir film followed by LB deposition at different surface pressures provides an efficient route to the generation of monolayers with tunable nanoparticle chain networks.

Conclusions

Extended assemblies of citrate-stabilized gold nanoparticles in the form of 2-dimensional chain networks are fabricated through the LB technique, the surface pressure providing a convenient handle to control the density of particles as well as the extension of the chains. The assembly process initiated by the adsorption of the negatively charged nanoparticles from the aqueous subphase on the Langmuir film formed by a cationic amphiphile monolayer at the air-water interface can be viewed as a novel mode of surface-catalyzed reaction. Kinetic investigations following the changes in the optical extinction of the subphase resulting from the assembly, reveal a Langmuir-Hinshelwood mechanism for the process. The LB deposition that captures the network assemblies provides a unique view of the surface-catalyzed reaction product.

Experimental Section

Synthesis

Gold nanoparticles were synthesized using the citrate reduction route.[41] 1.88 mL of a 0.085 M aqueous solution of trisodium citrate was added to 100 mL of a 0.24 mM aqueous solution of $HAuCl_4$ and maintained at 80°C with vigorous stirring for 1 h. The solution turned a clear ruby red. The gold nanoparticle solution obtained was kept at ambient temperature with stirring for 12 h. Analysis of the final nanoparticle solution by ICP-OES (Varian model 720-ES) showed the concentration of gold to be 0.267 mM (the minor increase with respect to the starting concentration may be attributed to the slight evaporation of the solution during the synthesis). Based on the absorbance of the LSPR at 520 nm, the extinction coefficient of the solution is estimated to be 3.5×10^3 M^{-1} cm^{-1}, equivalent to 2.9×10^8 M^{-1} cm^{-1} with the concentration expressed in terms of mols of nanoparticles (14 nm diameter) per liter, consistent with earlier reports.[53] High purity water (Millipore MilliQ, resistivity = 18.2 MΩ cm) was used in the synthesis. $ODEP^+Br^-$ was synthesized following reported procedure.[44]

Langmuir and LB film fabrication

A NIMA model 611M LB trough equipped with a Teflon® barrier and a Wilhelmy plate for pressure sensing was used to record the surface pressure-area (π-A) isotherm and fabricate the LB films; experiments were conducted in a clean environment with the temperature maintained at 22±1°C. Either high purity water or an aqueous solution of citrate-stabilized gold nanoparticles with concentration in the range 0.01 – 0.02 mM was used as the subphase. 70-80 μL of a 0.897 mM chloroform solution of $ODEP^+Br^-$ was spread on the surface. ~ 2 h was allowed for the complete evaporation of the solvent and homogeneous distribution of the amphiphiles on the surface. π-A isotherms were recorded at a barrier speed of 30 cm^2/min after the monolayers were subjected to a few isocycles to ensure consistency of the isotherm. The films are found to be quite stable up to pressures close to the collapse. LB films were deposited on quartz substrates with a hydrophilic surface (or copper grid fixed on glass plate) at selected surface pressures by vertical dipping at a speed of 3 mm/min.

Adsorption and assembly of nanoparticles on the Langmuir film

The experiments were carried out at 22±1°C. Required volumes of a 0.267 mM aqueous solution of gold nanoparticles were diluted to 150 mL with high purity water to prepare solutions with concentrations in the range 0.01 – 0.05 mM. Each solution was taken in a glass petri-dish (18 cm diameter). 85 μL of a 0.897 mM solution of $ODEP^+Br^-$ in chloroform was spread on the nanoparticle solution surface and the chloroform allowed to evaporate; the quantity of amphiphile molecules spread was estimated using the molecular area determined from the π-A isotherm in the LB experiment and the surface area of the solution in the petri-dish, so that a compact monolayer was formed at the air-solution interface. Extinction spectrum of the subphase was recorded using 3 mL samples collected before spreading the amphiphile and every 30 min afterwards, for up to 3 h; samples were collected with a syringe without disturbing the monolayer at the surface. Baseline of the spectrum was found to rise with time, especially for the higher initial concentrations of the subphase. The spectra were corrected for scattering and deconvoluted to estimate the intensity of the extinction due to the isolated gold nanoparticles (λ_{max} ~ 520 nm); plot of the corresponding concentration against time provides the rates of the nanoparticle assembly for the different initial concentrations.[40] Each experiment was repeated at least 3 times.

Characterization

Extinction/absorption spectra were recorded on a Varian model Cary 100 UV-visible spectrometer. A clean hydrophilic quartz plate or high purity water was used as the reference for recording the spectra of the LB film or nanoparticle solution respectively. TEM images of the LB film deposited on carbon-coated copper grids were recorded on an FEI Tecnai G^2 S-Twin TEM at an accelerating voltage of 200 kV. FE-SEM images of the LB films

on hydrophilic quartz plate were recorded on a Carl Zeiss model Merlin Compact 6027 FESEM with a beam voltage of 3.0 kV.

Analysis of nanoparticle chain networks

The TEM images were analyzed using the image analysis software, ImageJ Ver. 1.41o (W. Rasband, National Institute of Health, USA; Java 1.6.0_10). Particles in the image area (1×1 μm^2) were counted using the 'Cell Counter' option by marking each one and saving the coordinates. Using these coordinates and appropriate length scales, all interparticle distances were evaluated using a home-made computer program. Given a cut-off distance, the program constructs the particle connectivity list, defining the adjacency matrix, A of the equivalent simple graph.[54] $d_i = \sum_j A_{ij}$ provides the number of neighbors of each particle, *i*. The program then evaluates various powers of A; the smallest power, n for which $(A^n)_{ij} \neq 0$ defines the length of the shortest path between the points, *i* and *j* connected in the network. Distribution of the number of such paths of different lengths provides a quantitative representation of the chain network in the nanoparticle assembly.

Acknowledgements

Financial support from the Department of Science and Technology, New Delhi and infrastructure support from the Centre for Nanotechnology and the School of Chemistry at the University of Hyderabad are acknowledged with gratitude. We thank Mr. M. Durga Prasad for help with the TEM and FESEM imaging. LM thanks the UGC, New Delhi for an SRF.

Notes and References

School of Chemistry, University of Hyderabad - 500046, India
E- mail: tpr@uohyd.ac.in

Electronic supplementary information available (ESI): Details of experiments on the different amphiphile-metal nanoparticle combinations, details of the kinetics analysis and control experiments. See DOI 10.1039/b000000x/

1 R. Sardar, A. M. Funston, P. Mulvaney and R. W. Murray, *Langmuir,* 2009, **25**, 13840.
2 D. D. Evanoff Jr. and G. Chumanov, *ChemPhysChem,* 2005, **6**, 1221.
3 A. M. Funston, C. Novo, T. J. Davis and P. Mulvaney, *Nano Lett,* 2009, **9**, 1651.
4 M. Steiner, C. Debus, A. V. Failla and A. J. Meixner, *J. Phys. Chem. C*, 2008,**112***,* 3103.
5 S. A. Maier, P. G. Kik, H. A. Atwater, S. Meltzer, E. Harel, B. E. Koel and A. A. G. Requicha, *Nature Mater.*, 2003, **2**, 229.
6 S. Shaw and L. Cademartiri, *Adv.Mater*, 2013, **25**, 4829.
7 Z. Li, S. Butun and K. Aydin, *ACS Photonics,* 2014, **1**, 228.
8 T. Hui-Jung and L. Yuh-Lang, *Soft Matter,* 2009, **5**, 2962.
9 K. Heo, C. Miesch, T. Emrick and R. C. Hayward, *Nano Lett.*, 2013, **13**, 5297.
10 D. Orsi, A. Vezzani, R. Burioni, A. Pucci, G. Ruggeri and L. Cristofolini, *Colloids Surf. A*, 2014, **441**, 912.
11 E. Faoucher, P. Nativo, K. Black, J. B. Claridge, M. Gass, S. Romani, A. L. Bleloch and M. Brust, *Chem. Commun.*, 2009, 6661.
12 B. Pong, H. I. Elim, J. Chong, V. Ji, B. L. Trout and J. Lee, *J. Phys. Chem. C.*, 2007, **111**, 6281.
13 J. Liao, Y. Zhang, W. Yu, L. Xu, C. Ge, J. Liu and N. Gu, *Colloids Surf. A*, 2003, **223**, 177.
14 M. Li, S. Johnson, H. Guo, E. Dujardin and S. Mann, *Adv. Funct. Mater.*, 2011, **21**, 851.
15 S. Si, A. Kotal and T. K. Mandal, *J. Phys. Chem. C.*, 2007, **111**, 1248.
16 J. Zhang, J. Wang, X. Xu, H. Zhu, Z. Wang, F. Yang, B. Zhang and X. Yang, *Nanotechnology*, 2009, **20**, 295603-1.
17 G. Wang and R. W. Murray, *Nano Lett.*, 2004, **4**, 95.
18 L. Li and S. I. Stupp, *Angew. Chem. Int. Ed.*, 2005, **44**, 1833.
19 C. Song, M. G. Blaber, G. Zhao, P. Zhang, H. C. Fry, G. C. Schatz and N. L. Rosi, *Nano Lett.*, 2013, **13**, 3256.
20 R. S. Gill, R. F. Saraf and S. Kundu, *ACS Appl. Mater. Interfaces*, 2013, **5**, 9949.
21 X. Xiong, A. Busnaina, S. Selvarasah, S. Somu, M. Wei, J. Mead, C. Chen, J. Aceros, P. Makaram and M. R. Dokmeci, *Appl. Phys. Lett.*, 2007, **91**, 063101-1.
22 A. R. Tao, J. Huang and P. Yang, *Acc. Chem. Res.*, 2008, **41**, 1662.
23 C. R. Hansen, F. Westerlund, K. Moth, R. Ravindranath, S. Valiyaveettil and T. Bjørnholm, *Langmuir*, 2008, **24**, 3905.
24 N. Markovich, R. Olinsky and R. Jelinek, *J. Am. Chem. Soc.*, 2009, **131**, 2430.
25 H. Ma and J. Hao, *Chem. Eur. J.*, 2010, **16**, 655.
26 S. Kundu, *J. Appl. Phys.*, 2012, **112**, 014323-1.
27 W. Cheng, S. Dong and E. Wang, *J. Phys. Chem. B*, 2005, **109**, 19213.
28 L. Pei, K. Mori and M. Adachi, *Colloids Surf. A*, 2006, **281**, 44.
29 A. Morag, L. Philosof, R. Volinsky, E. Mentovich, S. Richter and R. Jelinek, *Adv. Mater.*, 2011, **23**, 4327.
30 B. P. Gagnon and M. –V. Meli, *Langmuir*, 2014, **30**, 179.
31 J. Paczesny, K. Sozanski, I. Dziecielewski, A. Zywocinski and R. Holyst, *J. Nanopart. Res.*, 2012, **14**, 826-1.
32 J. Huang, F. Kim, A. R. Tao, S. Connor and P. Yang, *Nature Mater.*, 2005, **4**, 896.
33 Y. Tatewaki, Y. Noda, T. Akutagawa, R. Tunashima, S. Noro, T. Nakamura, H. Hasegawa, S. Mashiko and J. Becher, *J. Phys. Chem. C*, 2007, **111**, 18871.
34 Y. Iwafuji and C. E. McNamee, *Colloids Surf. A*, 2012, **398**, 24.
35 A. A. Torrano, Â. S. Pereira, O. N. Oliveira Jr. and A. Barros-Timmons, *Colloids Surf. B* , 2013, **108**, 120.
36 F. Zhao, Y.-K. Du and J. -K. Xu, *Colloid J.*, 2009, **71**, 63.
37 D. I. Babenko, A. A. Ezhov, D. S. Turygin, V. K. Ivanov, V. V. Arslanov and M. A. Kalinina, *Langmuir*, 2012, **28**, 125.
38 H. Jia, X. Bai and L. Zheng, *CrystEngComm*, 2012, **14**, 2920.
39 K. Rajesh, B. Sreedhar and T. P. Radhakrishnan, *ChemPhysChem*, 2010, **11**, 1780.
40 See Supporting Information.
41 R. J. B. Pinto, P. A. A. P. Marques, M. A. Martins, C. P. Neto and T. Trindade, *J. Colloid Interface Sci.*, 2007, **312***,* 506.
42 M. S. Chandra and T. P. Radhakrishnan, *Mol. Cryst. Liq. Cryst.*, 2003, **403**, 77.
43 K. Rajesh, M. S. Chandra, S. Hirakawa, J. Kawamata and T. P. Radhakrishnan, *Langmuir*, 2007, **23**, 8560.
44 M. S. Chandra, Y. Ogata, J. Kawamata and T. P. Radhakrishnan, *Langmuir*, 2003, **19**, 10124.
45 J. S. Scildkraut, T. L. Penner, C. S. Willand and A. Ulman, *Opt. Lett.*, 1988, **13**, 134.
46 B. T. Ingram, R. H. Ottewill, in *Cationic Surfactants : Physical Chemistry*, eds. D. N. Rubingh, P. M. Holland, Marcel Dekker, New York, 1991, p. 87.
47 M. Sano, A. Kamino and S. Shinkai, *J. Phys. Chem. B.*, 2000, **104**, 10339.
48 P. C. Stenger, S. G. Isbell, D. St. Hillaire and J. A. Zasadzinski, *Langmuir*, 2009, **25**, 10045.
49 W. Cheng, S. Dong and E. Wang, *J. Phys. Chem. B*, 2005,**109**,19213.
50 A. Moores and F. Goettmann, *New J. Chem.*, 2006, **30**, 1121.
51 S. K. Ghosh and T. Pal, *Chem. Rev.*, 2007,**107**, 4797.
52 J. J. Mock, D. R. Smith and S. Schultz, *Nano Lett.*, 2003, **3**, 485.
53 X. Liu, M. Atwater, J. Wang and Q. Huo, *Colloids Surf. B*, 2007, **58**, 3.
54 F. Harary, *Graph Theory,* Narosa, New Delhi, 1988.

Text and graphics for the Table of Contents

Text

Negatively charged metal nanoparticles assemble as chain networks through Langmuir-Hinshelwood kinetics on a Langmuir film of positively charged amphiphiles. The extension of the networks captured in Langmuir-Blodgett films is tuned by the deposition pressure.

Graphics